(第3号様式) (Form No. 3)

学 位 論 文 要 旨
Dissertation Summary

氏　　名 (Name) Utari Sriwijaya Minaka

論 文 名:
(Dissertation Title) Assessment of Effectiveness and Design Procedure of Gravel Drains as Liquefaction Countermeasure

---

The current design practice of gravel drains as a liquefaction countermeasure involves selection of drain spacing and diameter to keep the peak excess pore water pressure ratio low, which was verified mostly with small scale 1g shaking tests; its validity for field scale prototype is yet to be well investigated. Seed and Booker (1977) suggested using a constant value of m_v irrespective of the excess pore pressure ratios and confining pressures in the design procedure. However, depending on the confining stress level, the variation of m_v can be more than several times the value of m_v, and thus, making m_v to be constant regardless of stress level or depth may not be a reasonable approach. Infinite permeability in the drain assumption was proposed in the design by Seed and Booker. Meanwhile, Onoue (1988) claimed the importance of the drain capacity to flow water, and proposed the importance of the well resistance to be taking into account in the design procedure.

In this study, a series of centrifuge tests was conducted to gain insight into the stress-dependent behavior of loose sand deposits with the level surface improved by gravel drains. The coefficient of volumetric compressibility, m_v, one of important features of mechanical properties of soils involved in the design of gravel drains was examined through triaxial cyclic tests. The permeability tests were conducted to examine the flow regime in the drain. Further, the current design procedures were validated with experimental data.

The model ground tested in this study was an 8m deep uniform sand deposit subjected to base shaking. The centrifuge models with and without gravel drains were implemented. Testing parameters, including the permeability of soils, the drain diameter, and the groundwater level,

were varied among tests to investigate their effects. The time histories of r_u for fully saturated models with gravel drains are demonstrated in Figure 1.

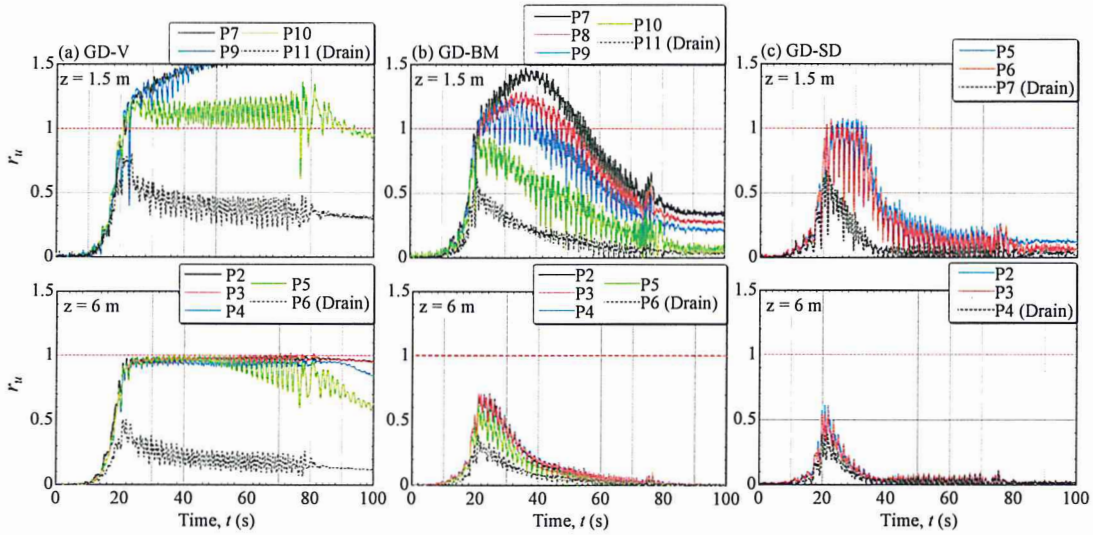

Figure 1 Pore pressure ratio time histories of the model with gravel drains

For the model GD-V, with 40 times lower permeability, r_u in sand at both shallower and deeper depths started to increase significantly at approximately t= 16s; the sand reached initial liquefaction at t= 20s and continued to liquefy throughout the shaking event. In the test GD-BM, r_u in sand at a greater depth (z= 6m) attained its maximum value of r_u= 0.4-0.7 at around t= 21s, then leveled off for some time from 21 to 25s, indicating dissipation balanced generation, which was followed by swift dissipation even during shaking. In contrast with r_u at the shallower depth (z= 1.5m) at any radial locations reached the liquefaction condition, although the effects of gravel drains can be observed on the timing of dissipation initiation, as well as in the form of dilative responses during shaking. At the shallower depth of z= 1.5m, sand did liquefy for GD-SD, regardless of the fact that compared to GD-BM, positive effects of the smaller drain diameter in the form of more significant dilative dips in pore pressure responses that appeared from the beginning of shaking, as well as swifter dissipation, can be observed in GD-SD.

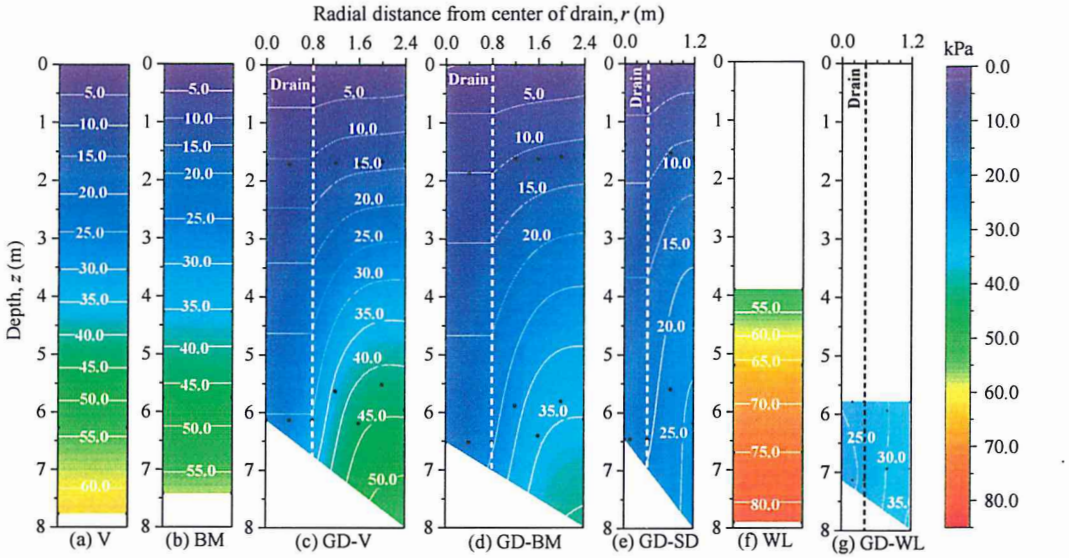

Figure 2 Contour graphs of excess pore pressure

To simultaneously examine the horizontal and vertical flow of the pore fluid, contours of the maximum excess pore pressure, Δu_{max}, attained at t= 21–22s for the centrifuge test without and with gravel drain are presented in Figure 2. For V and GD-V, the slopes and intervals of the contour lines at greater depth (z= 6m) demonstrate that the horizontal hydraulic gradient was high only at the perimeter of the gravel drain (r= 0.8–1.0m from the center of the gravel drain) but low at the zone with r> 1.2m. For model GD-BM, a zone with hydraulic gradients heading towards the drain extended radially to the midpoint, 2.4 m from the center of the drain; whereas, the excess pore pressures were kept lower than the companion model (BM). At a shallower depth, the slopes are gentle suggesting that the pore water did not flow toward the drain but the sand surface. Contours of GD-SD indicate that, at greater depth, the zone with hydraulic gradients heading towards drains extended radially to the midpoint (r= 1.2m). The contour line slopes are steep, with Δu_{max} lower than that at the corresponding points in GD-BM. r_{u_max} in sand of GD-WL is considerably lower than GD-SD. The dissipation in sand is more rapid for GD-WL than GD-SD.

A series of triaxial tests were performed to determine m_v value of the saturated sands under cyclic loading. The coefficient of volumetric strain, m_v (= $\varepsilon_v/\Delta u_t = \varepsilon_v r_u/\sigma_{c0}$') is considered to be inversely proportional to the initial effective confining pressure. The relationship between m_v and σ_{c0}' is demonstrated in Figure 3.

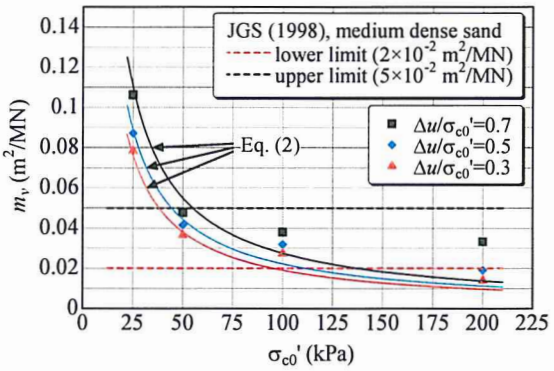

Figure 3 Relationship between m_v and effective confining pressure

Numerical simulations were performed in a finite difference scheme with the soil parameters obtained from the laboratory tests. The comparison of r_u in radial distribution from numerical simulation results and centrifuge test results for the model with drain are shown in Figure 4. Variations in r_{u_max} with depth also agree fairly well with those from the tests. The sand in the fully saturated ground near the ground surface always liquefies irrespective of the drain diameter and the permeability of soils while r_{u_max} at greater depth decreases with increasing soil permeability and drain diameter.

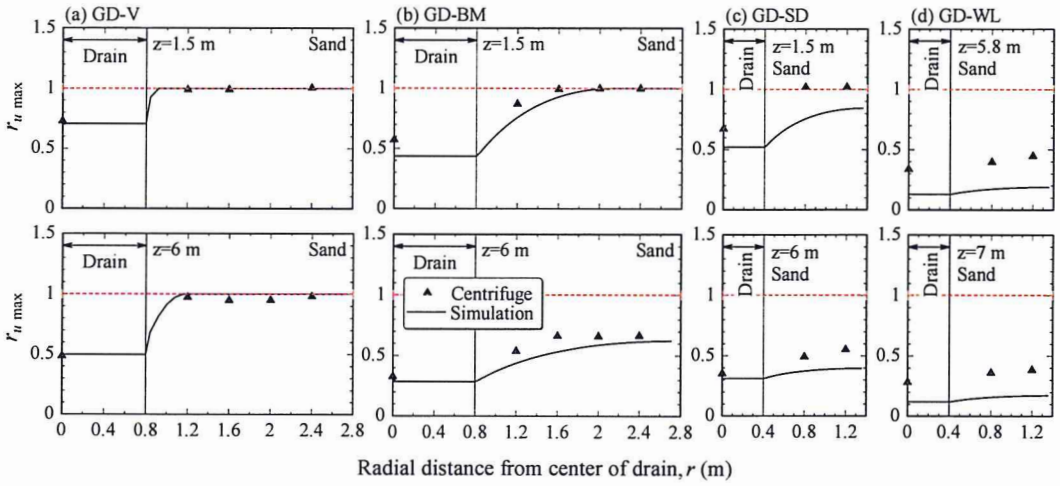

Figure 4 Comparisons of radial distributions of r_{u_max} from numerical analysis with the tests

This study revealed that the effects of gravel drains to suppress the excess pore pressures depend significantly on depth. The axisymmetric diffusion equation with consideration of well resistance appropriately predicts the excess pore pressures in sand with gravel drain when the stress level dependent m_v and Reynolds number dependent k_w are utilized for input soil parameters.

On 28th September 2018, an earthquake of M_w 7.5 hit the Central Sulawesi province in Indonesia. This was followed by liquefaction-induced large-scale ground flows in several areas in Palu city and its neighborhood. A significant characteristic of the ground flows at these sites was that large

volume of soil slid downhill along gentle topographic gradients and travelled long distances (more than several hundred meters). To gain a better understanding of the fundamental mechanisms contributing to ground flows, a site investigation conducted at Sibalaya, one of the sites where massive ground flows were observed. In situ tests, including eight large trench excavations and dynamic cone penetration tests, were carried out, which helped identify the liquefied and largely sheared layers. An analysis of the change in topography using satellite images and UAV photos also played an important role in capturing the overall picture of the event. Finally, a hypothesized mechanism for the extremely long slide was discussed.

Figure 5 shows the orthophotomap after the earthquake and photos of several locations. The easternmost margin of the affected area is bounded by the irrigation channel. Concrete panels were placed on the eastern side surface of the channel, while soil was exposed unlined on the bottom and western sides (b). In one southern breached channel section, a box culvert and a sluice gate were heavily damaged, which was most probably the cause of the extremely loud sound heard by the residents. Point (c) demonstrates the overview of inundation area. There were two major flow paths from the channel that created a cliff as high as several meters (d). In this area, as shown in (e), three large blocks were identified, with dimensions of the largest block as 80-m-long and 42-m-wide, that moved about 50 m downwards, which most possibly triggered the irrigation channel failure. Meanwhile, head scarps were formed along the western side of the channel (f).

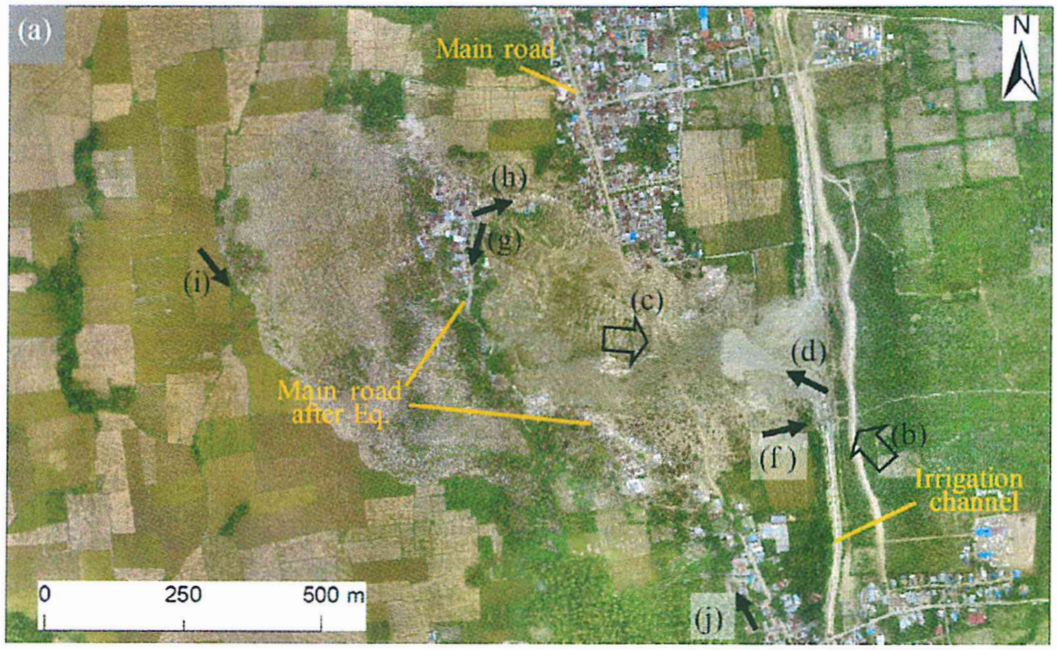

Figure 5 Orthophotomap after the earthquake

Figure 6 represents change in height in the flowslide and surrounding areas and locations of the trench. Consequently, the average subsidence over the entire flowslide is 0.25 m, while that of

the area outside the flowslide is also estimated to be 0.013 m, with the subsidence in the area in the east of irrigation channel being generally very small. Totally seven trenches were excavated in the flowslide as located in Figure 6.

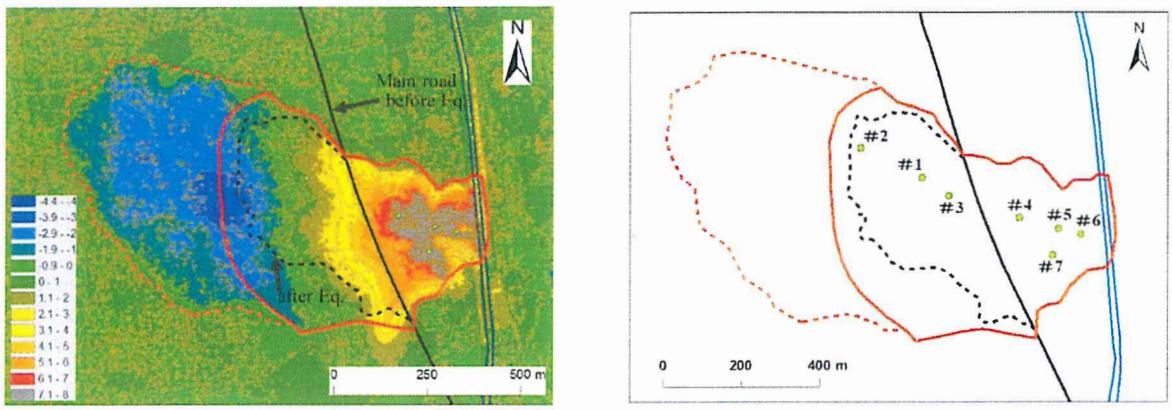

Figure 6 Elevation contour of the flow area (left) and locations of the trench (right)

Figure 7 depicts the cross-section A-A' along with the main stream of the flowslide passing through most trenches excavated in this study, together with depths of identified liquefied layers in each trench. The broken line represents a possible slip surface or a shear zone, along which large shear deformation is considered to have occurred, and soils above the line slid downslope while that underneath remained. The flowslide is the consequence of the shear resistance of the zone degrading significantly or being completely lost against the sliding deformation.

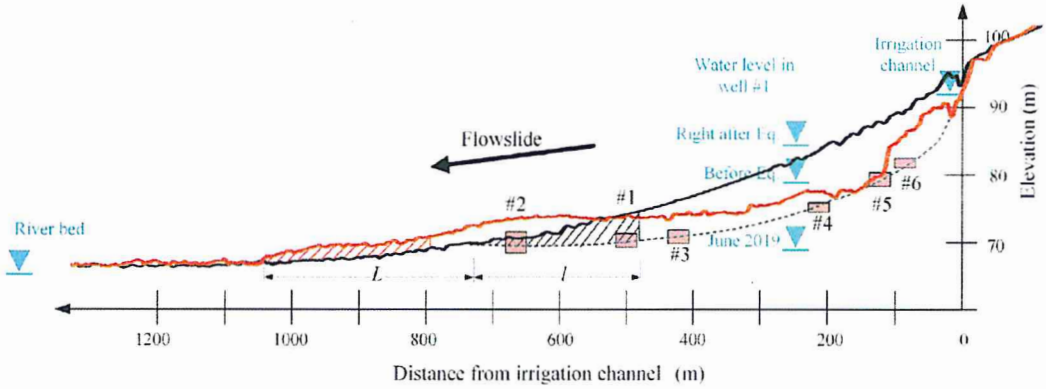

Figure 7 Cross section of A-A' section before and after the earthquake together with highly sheared depths detected in trenches